Springer

Journal of
Mechanical
Science and
Technology

Journal of Mechanical Science and Technology 22 (2008) 770~779

www.springerlink.com/content/1738-494x

Numerical simulation of droplet formation in a micro-channel using the lattice Boltzmann method

L. S. Kim, H. K. Jeong, M. Y. Ha* and K. C. Kim

School of Mechanical Engineering, Pusan National University, San 30, Jangjeon-Dong, Kumjung-Ku, Busan 609-735, Korea

(Manuscript Received April 25, 2007; Revised November 27, 2007; Accepted December 7, 2007)

Abstract

This study investigates droplet formation in a micro-channel using the lattice Boltzmann (LB) method. A cross-junction micro-channel and two immiscible, water and oil phase fluids, were used to form the micro-droplets. Droplets are formed by the hydrodynamic instability on the interface between two immiscible fluids when two immiscible fluids are imported simultaneously in a cross-junction micro-channel. The Shan & Chen model, which is a lattice Boltzmann model of two-phase flows, is used to treat the interaction between immiscible fluids. The detailed process of the droplet formation in the cross-junction micro-channel was illustrated. The results of the droplet formation by the LBM predicted well the experimental data by PIV (particle image velocimetry). The effect of the surface tension and the flow rate of water phase fluid on the droplet length and the interval between droplets was also investigated. As the surface tension increased, the droplet length and the interval between droplets were increased. On the other hand, when we increased the flow rate of the water phase fluid under the condition of the fixed oil-phase fluid flow rate, the droplet size was increased while the interval between droplets was decreased.

Keywords: Droplet formation; Micro channel; Two phase flow; Lattice Boltzmann method; Shan and Chen model

1. Introduction

Due to the rapid development of micro-electro-mechanical systems (MEMS) recently, many researchers have shown strong interest in microfluidics and have carried out many studies to apply the MEMS technology to microfluidic systems such as lab-on-a-chip and μ-TAS (Micro Total Analysis System). In particular, many researchers have shown a big interest in developing the technology to form micro-droplets in a micro-channel, because chemical reaction conditions can be controlled precisely by using the droplet-based structure, and chemical reactions with a constant diffusion distance can occur effectively in the micro-volume. As a result, the micro-droplet technology can make very sensitive chemical reactions, which was not possible in traditional chemical reactions, possibly with a minimum amount of reactants.

Micro-droplets have been used widely to increase the diffusion rates between the interfaces of two immiscible fluids and have many applications in the chemical and bio-chemical fields. Some experimental studies to investigate the characteristics of micro-droplets formed in the micro-channel have been reported [1-8].

Anna et al. [1] integrated a flow-focusing geometry into a microfluidic device and produced both monodisperse and polydisperse emulsions. Thorsen et al. [2] showed that a microfluidic device designed to produce reverse micelles can generate complex and ordered droplet patterns as it is continuously operated far from thermodynamic equilibrium. Tice et al. [3] characterized the conditions required to form nanoliter-sized droplets of viscous aqueous reagents in flows of immiscible carrier fluid within microchannels. They also showed that combining viscous

*Corresponding author. Tel.: +82 51 510 2440, Fax.: +82 51 515 3101
E-mail address: myha@pusan.ac.kr
DOI 10.1007/s12206-007-1201-8

and non-viscous reagents could enhance mixing in droplets moving through micro-channels by providing a nearly ideal initial distribution of reagents within each droplet. Burns and Ramshaw [4] demonstrated the enhancement of diffusion rate in a micro-droplet-based micro-reactor. Song et al. [5] described the rapid mixing and transportation of multiple solutions of reagents without dispersion by using water micro-droplets in an immiscible oil-phase fluid. Song and Ismagilov [6] described a microfluidic chip for performing kinetic measurements of micro-droplets with better than millisecond resolution. Song et al. [7] presented a microfluidic system used to control networks of many chemical reactions on the millisecond scale. Yoon and Kim [8] measured both internal and external flow fields in and around micro-droplets formed in the Y-junction micro-channel using the micro-PIV (particle image velocimetry) method. They suggested a method to measure the detailed fields of two-phase flow with deformable and moving boundaries.

Recently, the lattice Boltzmann (LB) method has been developed from the lattice-gas automata [9, 10]. The LB method has emerged as an alternative method for conventional computational schemes. Unlike conventional numerical methods based on the discretization of macroscopic continuum equations, the LB method is based on microscopic models and mesoscopic kinetic equation. The LB method recovers the Navier-Stokes equations in the incompressible flow limit. Since the LB method can be considered as a mesoscopic approach, lying in between microscopic molecular dynamics and conventional macroscopic fluid dynamics, it can be useful when microscopic statistics and macroscopic description of flow are important, e.g., in problems involving surface tension, capillarity and phase transition in multiphase multi-component systems [11].

There are some LB models for the multi-phase flows between immiscible fluids such as Rothman and Keller model [12], Shan and Chen model [13], etc. Particularly, the Shan and Chen [S-C] model, which was proposed to simulate the multi-component non-ideal gas, has been widely used to calculate the movement of the bubble (s) or the droplet (s) formed between the immiscible fluids.

Hou et al. [14] carried out a numerical study to compare the Rothman and Keller model and the S-C model to simulate a static bubble. They examined isotropy, strength of surface tension, thickness of the interface, spurious currents, Laplace's law, and steadiness of the bubble. They also showed that the S-C model could simulate a physically correct, isotropic and stable bubble formation satisfying Laplace's law, while the Rothman and Keller model was not good for representing the bubble formation. Sehgal et al. [15] simulated numerically the deformation and fragmentation of a liquid drop in a flow field using the S-C LB model. Yang et al. [11, 16] investigated the characteristics of bubble growth, detachment, and coalescence on vertical, horizontal, and inclined downward-facing surfaces using the S-C LB model. Yang et al. [17] also simulated the movement of Taylor bubbles in a narrow channel using the S-C LB model.

The present study investigates droplet formation in a micro-channel using the lattice Boltzmann (LB) method as a numerical method and S-C model to treat the interaction between immiscible fluids. A cross-junction micro-channel and two immiscible, water and oil phase fluids, are used to form the micro-droplets in the micro-channel. The detailed flow fields in and around the droplets are investigated, and the process of droplet formation between immiscible fluids in a cross-junction micro-channel is illustrated. The effect of the surface tension and the flow rate of water phase fluid on the droplet length and the interval between droplets is also investigated. The present prediction results for the droplet formation by the LBM are compared with the experimental data obtained by using the PIV technique.

2. Numerical method

2.1 Formulation of lattice boltzmann method

LB models are derived from the continuous Boltzmann equation with the collision term in the Bhatnagar-Gross-Krook (BGK) approximation. The original lattice Boltzmann equation is defined as

$$f_i^\sigma\left(\mathbf{x}+\hat{\mathbf{e}}_i\Delta t, t+\Delta t\right)-f_i^\sigma\left(\mathbf{x},t\right)=\Omega_i^\sigma \tag{1}$$

where f_i^σ is the single-particle density distribution function of direction i of phase σ, $\mathbf{x}$ is the directional vector of lattice node, and $\mathbf{e}_i$ means the microscopic velocity which represents the magnitude and directional vector of particles. The right-hand side in Eq. (1) is called the collision term, which expresses the collisions between the particles propagated at a previous time. This collision term is too complex to

solve analytically, so Bhatnagar et al. [18] simplified the collision terms by introducing single relaxation time of a fluid, τ, expressed as

$$\Omega_i^\sigma = -\frac{1}{\tau}\left(f_i^\sigma(\mathbf{x},t) - f_i^{\sigma,eq}(\mathbf{x},t)\right) \tag{2}$$

This is called as the lattice BGK equation. $f_i^{\sigma,eq}$ represents the equilibrium distribution function, expressed as.

$$f_0^{\sigma,eq} = \rho^\sigma w_0\left[1 - \frac{3(\mathbf{u}^\sigma)^2}{2c^2}\right] \tag{3}$$

$$f_i^{\sigma,eq} = \rho^\sigma w_i\left[1 + \frac{3(\hat{\mathbf{e}}_i\cdot\mathbf{u}^\sigma)}{c^2} + \frac{9(\hat{\mathbf{e}}_i\cdot\mathbf{u}^\sigma)^2}{2c^4} - \frac{3(\mathbf{u}^\sigma\cdot\mathbf{u}^\sigma)}{2c^2}\right] \tag{4}$$

where ρ^σ is the density of phase σ, $\mathbf{u}^\sigma$ is the velocity vector of phase σ, and w_i is a weighting factor depending on the lattice model used. c represents the propagation speed of particles moving between a lattice node and its nearest neighbors.

Fig. 1 shows a schematic diagram to indicate the velocity directions used in the present D2Q9 model. The D2Q9 lattice model has one velocity vector at the center which is at rest, four velocity vectors for orthogonal lattices, and four velocity vectors for diagonal lattices. The weighting factor w_i used in the present calculation is

$$\begin{aligned} &w_0 = 4/9 \quad \text{if} \quad i = 0 \\ &w_i = 1/9 \quad \text{if} \quad i = 2, 4, 6, 8 \\ &w_i = 1/36 \quad \text{if} \quad i = 1, 3, 5, 7 \end{aligned} \tag{5}$$

After we obtain the solution for f_i^σ, the values of macroscopic variables such as density and velocity of fluid are calculated as

$$\rho^\sigma = \sum_i f_i^\sigma \tag{6}$$

$$\rho^\sigma \mathbf{u}^\sigma = \sum_i \hat{\mathbf{e}}_i f_i^\sigma \tag{7}$$

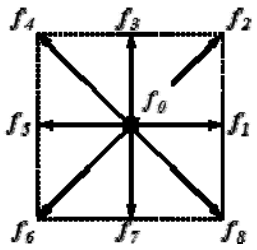

Fig. 1. A schematic diagram to show the velocity directions in the D2Q9 model.

In order to solve two-phase flow, we used the Shan and Chen model [13]. To model surface tension forces in multi-component fluids, the interaction potential $V(\mathbf{x},\mathbf{x}')$ can be incorporated [13]:

$$V(\mathbf{x},\mathbf{x}') = G_{\sigma\bar{\sigma}}(\mathbf{x},\mathbf{x}')\phi^\sigma(\mathbf{x})\phi^\sigma(\mathbf{x}') \tag{8}$$

where $\phi^\sigma(\mathbf{x})$ is an effective density function. $G_{\sigma\bar{\sigma}}(\mathbf{x},\mathbf{x}')$ in Eq. (8) is the interaction strength defined as

$$G_{\sigma\bar{\sigma}}(\mathbf{x},\mathbf{x}') = \begin{cases} 0, & |\mathbf{x}-\mathbf{x}'| > c \\ G_\sigma, & |\mathbf{x}-\mathbf{x}'| = c \end{cases} \tag{9}$$

The magnitude of G_σ in Eq. (9) controls the strength of the interaction potential between fluid components σ and $\bar{\sigma}$, while its sign determines whether it is attractive or repulsive. When we calculate the interaction potential $V(\mathbf{x},\mathbf{x}')$, we consider only the interactions between lattices located at the nearest neighbors shown in Fig. 1 to simplify the calculation. In the region of the single phase ($\sigma = \bar{\sigma}$), $G_{\sigma\bar{\sigma}} = 0$, whereas $G_{\sigma\bar{\sigma}} \neq 0$ in the region of multi-phase region ($\sigma \neq \bar{\sigma}$).

The total interaction force $\mathbf{F}^\sigma(\mathrm{x})$ on the σ th component at $(\mathbf{x})$ is determined as

$$\mathbf{F}^\sigma(\mathbf{x}) = -\phi^\sigma(\mathbf{x})\sum_{\sigma=1}^{S} G_{\sigma\bar{\sigma}}\sum_{i=0}^{b}\phi^{\bar{\sigma}}(\mathbf{x}+\hat{\mathbf{e}}_i)\,\hat{\mathbf{e}}_i \tag{10}$$

And the velocity of fluid is updated by the following Eqs. (11) and (12).

$$\rho^\sigma(\mathbf{x})\mathbf{u}^\sigma(\mathbf{x}) = \rho^\sigma(\mathbf{x})\bar{\mathbf{u}}(\mathbf{x}) + \tau^\sigma\mathbf{F}^\sigma \tag{11}$$

$$\bar{\mathbf{u}}(\mathbf{x}) = \left(\sum_{\sigma=1}^{S}\frac{1}{\tau^\sigma}\sum_{i=0}^{b} f_i^\sigma\hat{\mathbf{e}}_i\right)\Bigg/\left(\sum_{\sigma=1}^{S}\frac{1}{\tau^\sigma}\sum_{i=0}^{b} f_i^\sigma\right) \tag{12}$$

where the composite velocity $\bar{\mathbf{u}}(\mathbf{x})$ represents the flow of the bulk fluid and is the more meaningful velocity to view and analyze the overall fluid flow of the system.

In the lattice Boltzmann method, the kinematic viscosity of fluid can be expressed as

$$\nu^\sigma = \frac{2\tau^\sigma - 1}{6} \tag{13}$$

where τ^σ is the relaxation time of the σ th component [13].

2.2 Laplace's law

There is a pressure difference between the inside

and outside of bubbles and droplets. The pressure difference Δp depends on the radius of curvature R and the surface tension σ for the fluid pair of interest. For two-dimensional droplets and bubbles there is only one possible radius of curvature, and Laplace's law indicates that the pressure difference between the inside and outside of the bubble is linearly proportional to the reciprocal of bubble radius $(\Delta p = \sigma / R)$ [11].

3. Numerical results

In order to represent the capability of the lattice Boltzmann method for two-phase flow of the immiscible fluids, Yang et al. [11] demonstrated that the density change across the interface can be captured well and the Laplace's law is represented quite well by using the lattice Boltzmann simulation. The LBM code developed in this work is validated by using results illustrated by Yang et al. [11] as a benchmark test.

Fig. 2 shows the density distribution of two immiscible fluids for three different lattices of 50×50, 100×100 and 200×200, when G_σ = 0.05. It is shown that the computational domain is normalized with a scale of 1×1 for three different lattices, and a bubble has a static size of 0.3 in radius, and the density of each phase fluid is initially $\rho^\sigma = 1$. The contour of density distribution of two immiscible fluids in the whole computational domain is shown in Fig. 2(a). The density distributions of two immiscible fluids along the central line in the horizontal direction from the center point of the static bubble to the boundary of the computational domain are represented in Fig. 2(b). Figs. 2(a) and (b) illustrate that the interface between two immiscible fluids becomes narrower as the lattice number is increased, and also the density gradient across the interface can be captured for three different lattices.

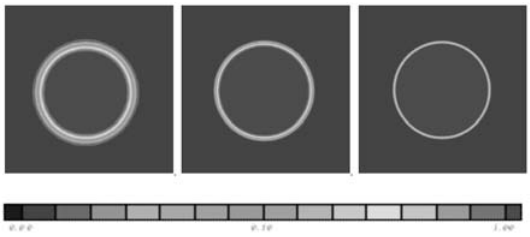

(a) The contour of density distribution for different lattices (from left, lattice 50×50, 100×100, 200×200)

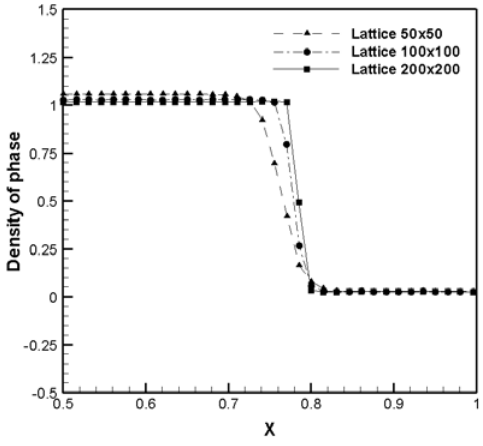

(b) Density distribution of bubble phase across the interface

Fig. 2. Density distribution for different lattices used when G_σ = 0.05.

As shown in Fig. 3, it is found that Laplace's law for the formed bubbles obtained by the lattice Boltzmann simulation is satisfied quite well. The present results are in good agreement with the results given by Yang et al. [11].

Fig. 4 shows the surface tension of two-phase flow as a function of G_σ with $\tau^\sigma = 1$, $\rho^\sigma = 1$ and 100×100 lattice. According to Laplace's law, the slope between the pressure difference Δp and the curvature $1/R$ means the surface tension as shown in Fig. 3. Therefore, Fig. 4 shows the variation of the surface tension with respect to an increase in the interaction potential parameter G_σ in this model. The surface tension increases almost linearly as a function of interaction potential parameter G_σ.

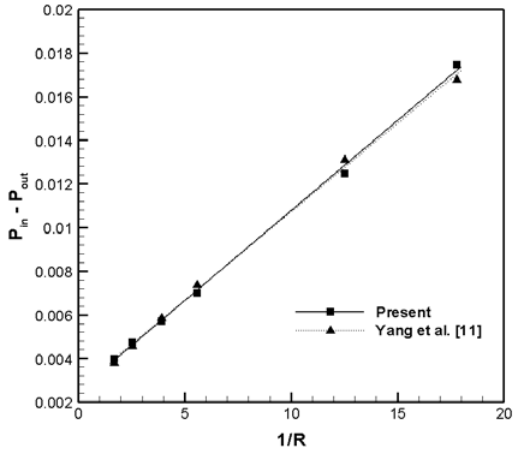

Fig. 3. Comparison of the present results with Yang et al. [11] for the pressure difference as a function of the curvature of bubble with $\tau^\sigma = 1$, $\rho^\sigma = 1$, $G_\sigma = 0.05$ and 100x100 lattice.

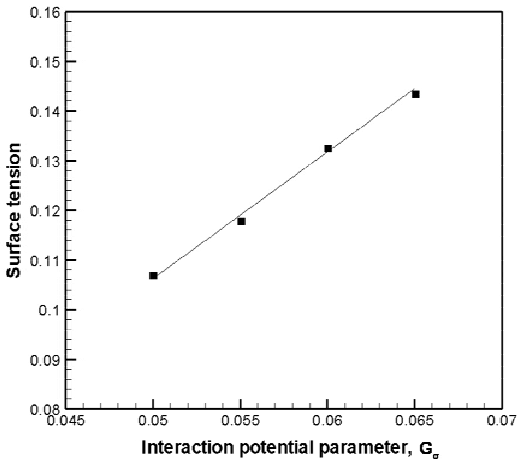

Fig. 4. Surface tension of two-phase flow as a function of G_σ with $\tau^\sigma = 1$, $\rho^\sigma = 1$ and 100×100 lattice.

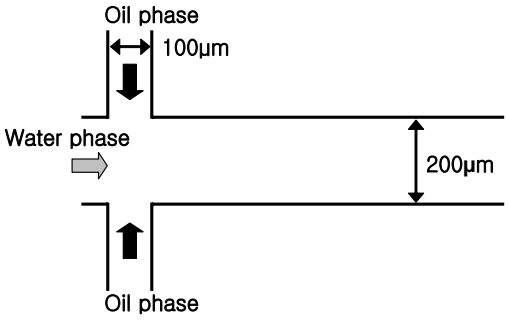

Fig. 5. A schematic diagram of a cross-junction micro-channel.

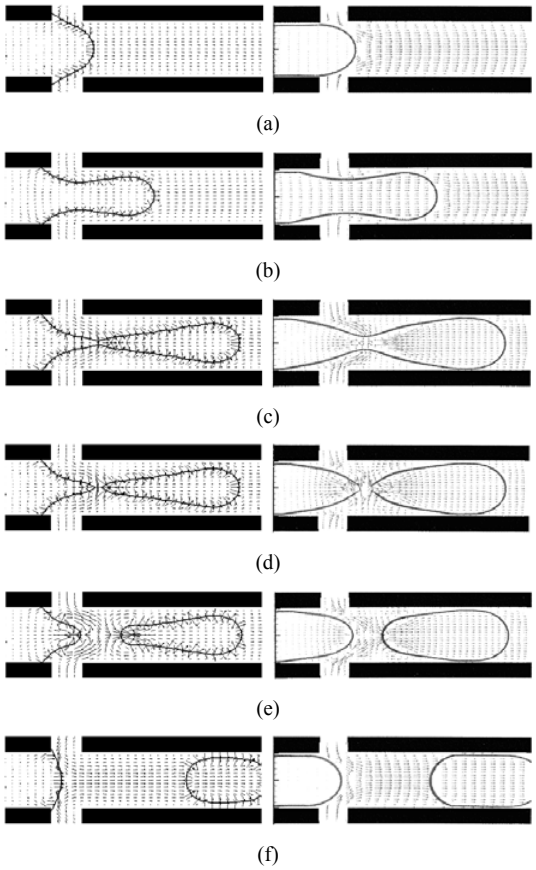

Fig. 6. Comparisons of the present predicted results (left side) with the PIV experimental data (right side) for the instantaneous flow fields of droplet formation with $\dot{V}_{oil}$ = 1.5 $\mu\ell$/min, $\dot{V}_{water}$ = 0.5 $\mu\ell$/min, G_σ = 0.085: (a)-(b) droplet growth, (c) extension, (d) separation, and (e)-(f) stabilization.

A schematic diagram of a cross-junction micro-channel used in this work is shown in Fig. 5. Inlet width for the water and oil phase fluids is 200 and 100 ㎛, respectively. The volumetric flow rate of the water phase fluid is changed from 0.5 to 1.0 $\mu\ell$/min. The volumetric flow rate of the oil phase fluid is fixed as 1.5 $\mu\ell$/min. Thus, the Reynolds number used in this study for the water and oil phase fluid flows is very small whose values are Re<0.01. Droplets are digitized when the water phase and the oil phase fluids flow into the cross-junction micro-channel.

For the present LB simulation, we used the inlet boundary condition at the entrance of each phase fluid and the outlet boundary condition at the outlet of right side, respectively. Using the initial value of density and velocity, $f_i^{\sigma,eq}$ is calculated by Eqs. (3) and (4), and then $f_i^\sigma = f_i^{\sigma,eq}$ is applied as initial and inlet boundary conditions. In order to reproduce the no-slip condition, the bounce-back boundary condition is adopted on the wall of the cross-junction micro-channel.

Fig. 6 shows a comparison of the present predicted results with the PIV experimental data [19] for instantaneous flow fields during the process of droplet formation when $\dot{V}_{oil}$ = 1.5 $\mu\ell$/min, $\dot{V}_{water}$ = 0.5 $\mu\ell$/min and G_σ = 0.085. The predicted and experimental results are shown in the left and right sides of Fig. 6, respectively. Here the volumetric flow rates of oil and water phases are 1.5 and 0.5 $\mu\ell$/min, respectively. It is shown that the droplet of water phase fluid grows, extends and finally separates due to the hydrodynamic instability on the interface between the water phase and the oil phase fluids; then, the droplet of water phase fluid is finally generated. This process is repeated and the droplets that have constant shapes

and sizes are regularly formed. The distribution of velocity vectors obtained by the present lattice Boltzmann method represents generally well the experimental data obtained by PIV, as illustrated in Fig. 6.

Figs. 6(a) and (b) show the growth and extension of the water phase fluid during the process of droplet formation. At first, the water phase fluid is smoothly imported into the micro-channel from the left side of a micro-channel. Next, while the water phase fluid is supplied into the micro-channel continuously, the droplet of water phase fluid grows and extends. Moreover, the neck of the droplet is gradually constricted due to more inflow of the oil phase fluid as shown in Fig. 6(c). And in Fig. 6(d), the section area near the droplet neck decreases abruptly and the inflow of the oil phase fluid increases rapidly. Figs. 6(e) and (f) show that the shape and movement of the separated droplet have become stable and the water phase fluid begins to grow to make the next droplet.

More detailed processes of the droplet movement to stabilization from separation in a cross-junction micro-channel are shown in Fig. 7. The left and right sides of Fig. 7 show the velocity vectors and streamlines, respectively. A droplet is separated from the water phase fluid (Fig. 7(a)), and then abrupt movement happens in the rear of the droplet in order to form the stable shape of the droplet due to the surface tension (Figs. 7(b)-(f)). Fig. 7(b) represents that vortices occur in the front of the water phase fluid and rear of the droplet, due to the recovery forces of the droplet and the water phase fluid. Two kinds of vortices in the rear of the droplet separated from the water phase fluid appear as shown in Figs. 7(b)-(d). One is a vortex toward the water phase fluid; this vortex reacts as a power to push the water phase fluid backward. The other is a vortex toward the rear of the droplet; this vortex causes the droplet to be stable rapidly. It is also seen that the internal velocity in the rear of the droplet is faster than that in the front of it up to taking the complete shape of a droplet (Figs. 7(e)-(g)). And inverse flow in the front of the water phase fluid is formed to build up the stabilized shape due to the interfacial tension between two immiscible fluids as shown in Figs. 7(d)-(g). After some more deformation, the droplet with a constant shape becomes stable and moves along the micro-channel with a constant velocity finally as shown in Fig. 7(h)-(j).

Surface tension is an important and dominant parameter to govern the movement of Taylor bubbles,

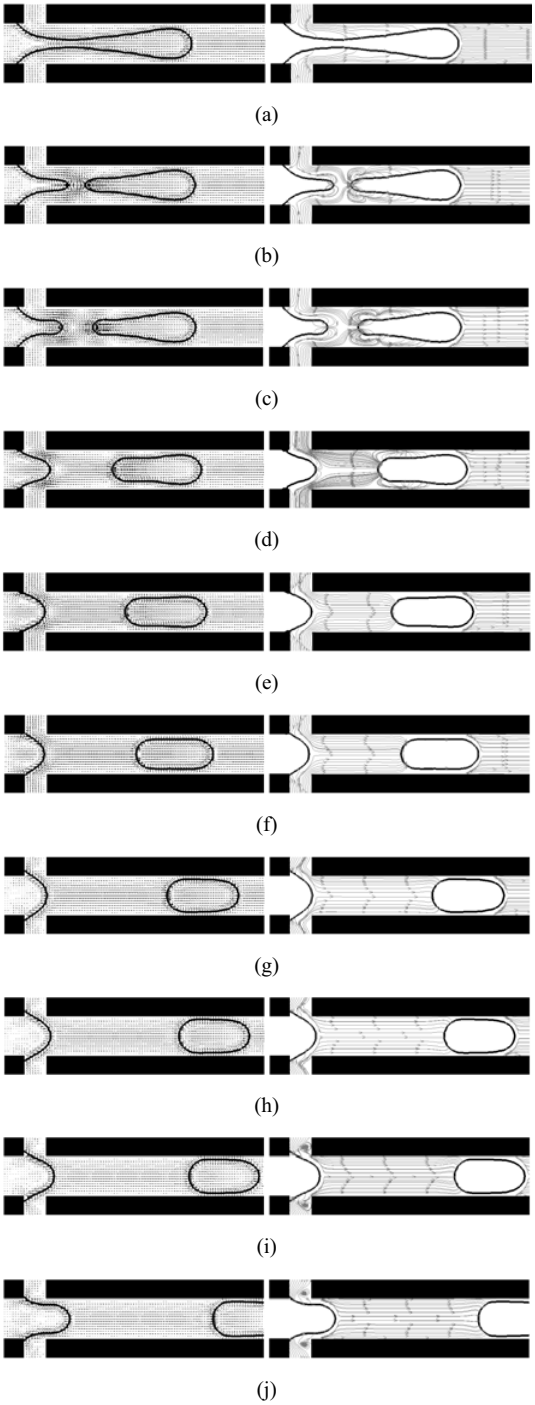

Fig. 7. Instantaneous velocity vectors and streamlines to show the process of the water droplet movement from separation to stabilization with $\dot{V}_{oil}$ = 1.5 $\mu\ell$/min, $\dot{V}_{water}$ =1.0 $\mu\ell$ /min, G_σ = 0.085: (a) instant separated, (b)-(h) deformation to be stable, (i)-(j) stabilization.

especially, in a narrow channel [17]. So the effect of surface tension on the droplet formation in the cross-junction micro-channel is investigated by changing the interaction potential parameter (G_σ) used in the present S-C LB model.

Figs. 8 and 9 show the variation of the length rate (DL/L) and the interval rate (DI/L) between the generated droplets as a function of the interaction potential parameter, where DL, DI and L represent the droplet length, the interval between the generated droplets and the inlet width for the water phase fluid, respectively. A longer time for droplet separation is required due to the increase of the cohesive force in the water phase fluid when the interaction potential becomes larger. Thus, it is shown that the droplet length and interval rates are almost linearly increased as the interaction potential parameter is increased. Fig. 10 shows the droplet formation obtained from the present computations by using the lattice Boltzmann method for different G_σ values of 0.05, 0.065 and 0.08 0.08. As shown in this figure, the droplet length and the interval between the generated droplets gradually increase as the interaction potential parameter (surface tension coefficient) increases.

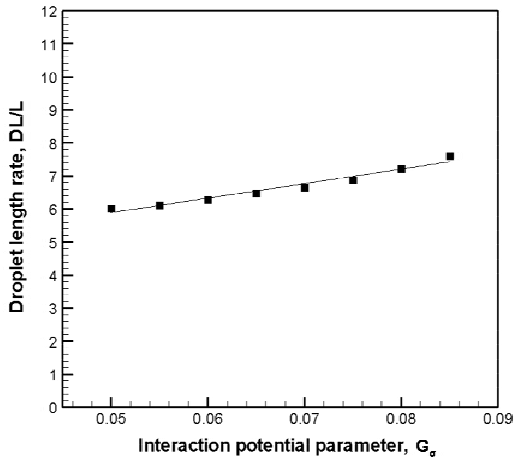

Fig. 8. Droplet length rate as a function of the interaction potential.

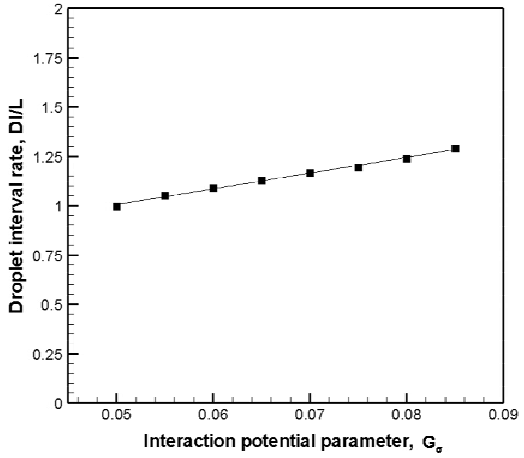

Fig. 9. Droplet interval rate as a function of interaction potential.

Fig. 11 shows a comparison of the present predicted results ((a), (c)) with the PIV experimental data ((b), (d)) for the droplet formation in the micro-channel with G_σ = 0.08 for the fixed oil-phase fluid flow rate of 1.5 $\mu\ell$/min and two different water-phase fluid flow rates of 0.5 and 1.0 $\mu\ell$/min. Droplets obtained by the present simulation are formed with constant droplet length and interval between droplets, and the present results for the droplet formation obtained by the lattice Boltzmann simulation reproduce generally well the experimental results obtained by PIV technique.

Figs. 12 and 13 show the droplet length rate and droplet interval rate, respectively, as a function of the water-phase fluid flow rate with $\dot{V}_{oil}$ = 1.5 $\mu\ell$/min for different interaction potential parameters of 0.08 and 0.085. The experimental data are also shown in Figures 12 and 13. The droplet length rate increases as the flow rate of the water phase fluid increases. On the other hand, the interval between droplets gradually decreases as the flow rate of the water phase fluid increases. The present computational results represent the PIV experimental data reasonably well, as shown in these figures.

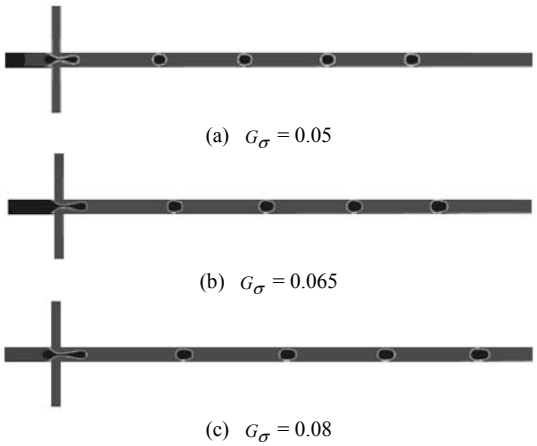

Fig. 10. Droplet formation for different interaction potentials of 0.05, 0.065 and 0.08.

(a) Present result

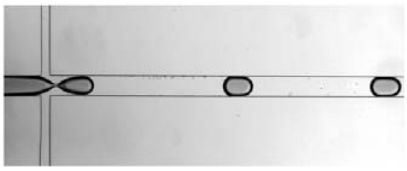

(b) Experimental result
($\dot{V}_{oil}$ = 1.5 $\mu\ell$ / min , $\dot{V}_{water}$ = 0.5 $\mu\ell$ / min)

(c) Present result

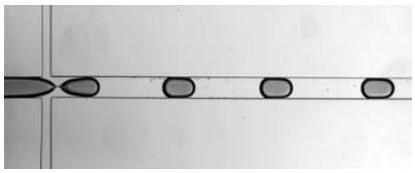

(d) Experimental result
($\dot{V}_{oil}$ = 1.5 $\mu\ell$ / min , $\dot{V}_{water}$ = 1.0 $\mu\ell$ / min)

Fig. 11. Comparison of the present predicted results ((a), (c)) with the experimental data ((b), (d)) for the droplet formation in the micro-channel with G_σ = 0.08.

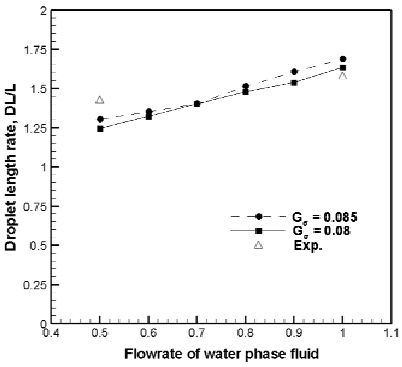

Fig. 12. Droplet length rate (DL/L) as a function of the water-phase fluid flow rate with $\dot{V}_{oil}$ = 1.5 $\mu\ell$/min for different interaction potentials of 0.08 and 0.085.

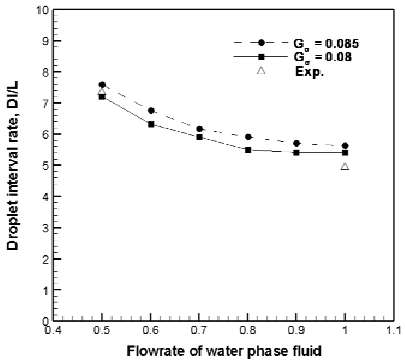

Fig. 13. Droplet interval rate (DI/L) as a function of the water-phase fluid flow rate with $\dot{V}_{oil}$ = 1.5 $\mu\ell$/min for different interaction potentials of 0.08 and 0.085.

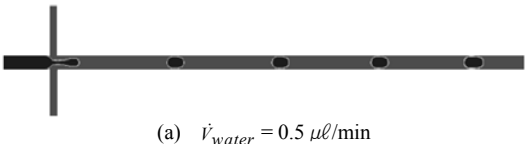

(a) $\dot{V}_{water}$ = 0.5 $\mu\ell$/min

(b) $\dot{V}_{water}$ = 0.7 $\mu\ell$/min

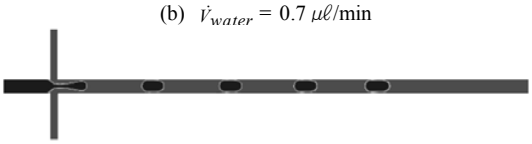

(c) $\dot{V}_{water}$ = 1.0 $\mu\ell$/min

Fig. 14. Droplet formation for different water-phase fluid flow rates of 0.5, 0.7 and 1.0 $\mu\ell$/min with $\dot{V}_{oil}$ = 1.5 $\mu\ell$/min and G_σ = 0.085.

Fig. 14 shows the droplet formation for different water-phase fluid flow rates of 0.5, 0.7 and 1.0 $\mu\ell$ /min when $\dot{V}_{oil}$ = 1.5 $\mu\ell$/min and G_σ = 0.085. When the volumetric flow rate of water phase fluid increases, the size of the formed droplets gets larger and the time period of the droplet formation decreases, because the velocity of the water phase fluid becomes faster under the condition of the fixed volumetric flow rate of the oil phase fluid.

4. Conclusions

The lattice Boltzmann method for two-phase flow has been applied in this work to simulate droplet formation between the immiscible fluids of water and oil phase fluids, when two immiscible fluids are simultaneously imported into a cross-junction micro-channel.

The process of droplet formation between two immiscible fluids in a cross-junction micro-channel is investigated. It is shown that the droplet of water phase fluid grows, extends and finally separtes due to the hydrodynamic instability on the interface between the water and oil phase fluids, and then a droplet of water phase fluid is generated. A constant moving velocity is finally established when the shape and movement of the droplet is stabilized. This process is repeated and the droplets with constant shapes and sizes are regularly formed. Present results obtained by the present lattice Boltzmann simulation represent generally well the experimental results obtained by the PIV technique.

The effect of the surface tension coefficient on the droplet length rate and the interval rates between the formed droplets has been investigated by changing the interaction potential parameters. When the interaction potential becomes larger, a longer time for droplet separation is required because the cohesive force in the water phase fluid increases. Thus, the droplet length rate and the formed interval rate increase linearly as a function of the interaction potential parameter (surface tension coefficient).

The droplet length rate increases with an increase in the flow rate of the water phase fluid. On the other hand, the interval between droplets gradually decreases as the flow rate of the water phase fluid increases. The present results for the droplet length rate and the interval rate of the generated droplets obtained by the LB simulation represent generally well the experimental results obtained by the PIV techniques.

5. Aknowledgment

This work was supported by the Korea Foundation for International Cooperation of science & Technology (KICOS) through a grant provided by korean Ministry of Science & Technology (MOST) in 2008 (No. k20702000013-07E0200-01310).

Nomenclature

$\hat{\mathbf{e}}$: Lattice speed, m/s
f : Distribution function
$\mathbf{F}$: Force, N
G : Interaction strength
P : Pressure, N/m^2
R : Droplet radius, m
t : Time, s
u : Velocity, m/s
x : Coordinates, (x, y), m
DL : Droplet length
DI : Droplet interval
L : Inlet width for the water phase fluid
$\dot{V}$: Volumetric flow rate

Greek symbols

v : Kinematic viscosity, m^2/s
ρ : Density, kg/m^3
τ : Relaxation time
ψ : Effective number density
σ : Surface tension, N/m

Superscript and subscripts

a : Index of discrete lattice velocity
b : The number of the discrete velocities
c : Critical value
eq : Equilibrium
S : The number of phases
σ : Index of phase, surface tension

References

[1] S. L. Anna, N. Bontoux and H. A. Stone, Formation of dispersions using “flow focusing” in microchannels, Applied Physics Letters 82 (2003) 364-366.
[2] T. Thorsen, R. W. Roberts, F. H. Arnold and S. R. Quake, Dynamic pattern formation in a vesicle-generating microfluidic device, Physical Review Letters 86 (2001) 4163-4166.
[3] J. D. Tice, A. D. Lyon and R. F. Ismagilov, Effects of viscosity on droplet formation and mixing in microfluidic channels, Analytica Chimica Acta 507 (2004) 73-77.
[4] J. R. Burns and C. Ramshaw, The intensification of rapid reactions in multiphase systems using flow in capillaries, Lab on a chip 1 (2001) 10-15.
[5] H. Song, M. R. Bringer, J. D. Tice, C. J. Gerdts and R. F. Ismagilov, Experimental test of scaling of mixing by chaotic advection in droplets moving through microfluidic channels, Applied Physics Letters 83 (2003) 4664-4666.
[6] H. Song and R. F. Ismagilov, Millisecond kinetics on a microfluidic chip using nanoliters of reagents, *J. AM. Chem. Soc*. 125 (2003) 14613-14619.
[7] H. Song, J. D. Tice and R. F. Ismagilov, A micro-

fluidic system for controlling reaction networks in time, Angew. Chem. Int. Ed. 42 (2003) 767-772.

[8] S. Y. Yoon and K. C. Kim, Micro-PIV measurement of water/oil two phase flow in a Y-junction microchannel, 5th International symposium on Particle Image Velocimetry (2003).

[9] U. Frisch, B. Hasslacher and Y. Pomeau, Lattice gas automata for Navier-Stokes equation, Physical Review Letters 56 (1986) 1505-1508.

[10] H. Chen, S. Chen and W. H. Matthaeus, Recovery of the Navier-Stokes equations using a lattice-gas Boltzmann method, Physical Review A 45 (1992) 5339-5342.

[11] Z. L. Yang, T. N. Dinh, R. R. Nourgaliev and B. R. Sehgal, Numerical Investigation of bubble growth and detachment by the lattice-Boltzmann method, *Int. J. of Heat and Mass Transfer* 44 (2001) 195-206.

[12] D. H. Rothman and J. Keller, Immiscible cellular-automaton fluids, J. Stat. Physics 52 (1998) 1119-1127.

[13] X. Shan and H. Chen, Lattice-Boltzmann model for simulating flows with multiple phases and components, Physical Review E 47 (1993) 1815-1819.

[14] S. Hou, X. Shan, Q. Zou, G. D. Doolen and W. E. Soll, Evaluation of two lattice Boltzmann models for multiphase flows, *J. of comp. physics* 138 (1997) 695-713.

[15] B. R. Sehgal, R. R. Nourgaliev and T. N. Dinh, Numerical simulation of droplet deformation and break-up by lattice-Boltzmann method, Progress in Nuclear Energy 34 (1999) 471-488.

[16] Z. L. Yang, T. N. Dinh, R. R. Nourgaliev and B. R. Sehgal, Numerical investigation of bubble coalescence characteristics under nucleate boiling condition by a lattice-Boltzmann model, *Int. J. Therm. Sci*. 39 (2000) 1-17.

[17] Z. L. Yang, B. Palm and B. R. Sehgal, Numerical simulation of bubbly two-phase flow in a narrow channel, *Int. J. of Heat and Mass Transfer* 45 (2002) 631-639.

[18] P. Bhatnagar, E. Gross and M. Krook, A model for collision processes in gases. I. Small amplitude processes in charged and neutral one-component systems, Physical Review 94 (1954) 511-525.

[19] S. Y. Yoon, Comprehensive methods of concentration and 3D flow field measurement for single/two phase micro total analysis system, Ph.D. Thesis, Pusan National University, (2005).